



University of Dundee

Stabilizing interaction of exopolymers with nano-Se and impact on mercury immobilization in soil and groundwater

Wang, Xiaonan; Song, Wenjuan; Qian, Haifeng; Zhang, Daoyong; Pan, Xiangliang; Gadd, Geoffrey Michael

Published in:
Environmental Science: Nano

DOI:
[10.1039/c7en00628d](https://doi.org/10.1039/c7en00628d)

Publication date:
2018

Document Version
Peer reviewed version

[Link to publication in Discovery Research Portal](#)

Citation for published version (APA):

Wang, X., Song, W., Qian, H., Zhang, D., Pan, X., & Gadd, G. M. (2018). Stabilizing interaction of exopolymers with nano-Se and impact on mercury immobilization in soil and groundwater. *Environmental Science: Nano*, 5(2), 456-466. <https://doi.org/10.1039/c7en00628d>

General rights

Copyright and moral rights for the publications made accessible in Discovery Research Portal are retained by the authors and/or other copyright owners and it is a condition of accessing publications that users recognise and abide by the legal requirements associated with these rights.

- Users may download and print one copy of any publication from Discovery Research Portal for the purpose of private study or research.
- You may not further distribute the material or use it for any profit-making activity or commercial gain.
- You may freely distribute the URL identifying the publication in the public portal.

Take down policy

If you believe that this document breaches copyright please contact us providing details, and we will remove access to the work immediately and investigate your claim.

1 **Stabilizing Interaction of Exopolymers with Nano-Se and Impact on Mercury**

2 **Immobilization in Soil and Groundwater**

3 Xiaonan Wang^{a,c}, Wenjuan Song^a, Haifeng Qian^{a,b}, Daoyong Zhang^{a,b}, Xiangliang

4 Pan^{a,b,*} Geoffrey Michael Gadd^d

5 ^a*Xinjiang Key Laboratory of Environmental Pollution and Bioremediation, Xinjiang*

6 *Institute of Ecology and Geography, Chinese Academy of Sciences, Urumqi 830011,*

7 *China*

8 ^b*College of Environment, Zhejiang University of Technology, Hangzhou 310014,*

9 *China*

10 ^c*University of Chinese Academy of Sciences, Beijing 100049, China*

11 ^d*Geomicrobiology Group, School of Life Sciences, University of Dundee, Dundee*

12 *DD15EH, Scotland, UK*

13 *For correspondence. E-mail panxl@zjut.edu.cn; Tel. +86 571 88320634; Fax +86

14 571 88320634.

15

16 **Running title:** EPS enhance mercury remediation by SeNPs

17

18 **ABSTRACT**

19 Remediation of metal-contaminated soils and waters using nanoparticles is
20 highly limited by their strong tendency to aggregate in soil solution and natural water.
21 In order to enhance remediation of Hg⁰ contaminated soil solution and groundwater
22 by SeNPs (Se nanoparticles), the effects of extracellular polymeric substances (EPS)
23 on the stability of SeNPs and Hg⁰ removal were investigated. EPS from the selenite-
24 reducing bacterium *Citrobacter freundii* Y9 was found to make SeNPs more
25 negatively charged by strong adsorption which significantly enhanced the stability
26 of SeNPs. The protein, carboxylate, polysaccharide and lipid components of the EPS
27 were involved in the adsorption to SeNPs. Fluorescence quenching titration
28 measurements implied that the binding of proteinaceous substances in the EPS to
29 SeNPs was static quenching. EPS can therefore enhance the remediation efficiency
30 of SeNPs for soil solution and groundwater contaminated with Hg⁰. This study
31 highlights that bacterial EPS can be used as an effective natural dispersant for SeNPs
32 therefore improving the efficiency of mercury immobilization in contaminated
33 waters.

34 **Keywords:** Aggregation; dispersant; EPS; fluorescence quenching titration;
35 remediation; mercury; selenium

36

37 **Introduction**

38 Nanoparticles have received considerable attention for their potential
39 application in the remediation of metal-contaminated sites because of their high
40 chemical and biological reactivity.¹ However, remediation of contaminated soils and
41 waters using nanomaterials is highly challenging because there is a strong tendency
42 for agglomeration of nanoparticles in the soil or sediment solutions which results in
43 limited dispersion and thus substantially reduces the remediation performance.
44 Moreover, nanoparticles readily anchor onto various solid matrices in soil. It is
45 therefore of great importance to maintain the dispersion properties of nanoparticles.

46 Two approaches have been proposed to improve dispersion of nanoparticles:
47 steric and electrostatic stabilization.² Steric stability can be provided by dispersants
48 which tightly bind to the nanoparticle surface and surface charge can be imparted or
49 increased to enhance electrostatic repulsion. Some studies have shown that
50 dispersants can significantly improve nanoparticle stability and mobility in both
51 water and soil.^{3,4} However, the wide use of chemically produced polymeric
52 dispersants provides another challenge to the environment. Therefore, it is desirable
53 to seek natural and environmentally-friendly dispersants to stabilize nanoparticles.

54 Some natural organic matter (NOM), such as humic substances, can increase
55 electrostatic repulsion or steric stability of nanoparticles by binding to the
56 nanoparticles which subsequently modifies their surface chemistry and charge.⁵

57 However, effects of NOM on the stability of nanoparticles reported in the literature
58 are contradictory. Some studies showed that organic matter contributes to the
59 formation of densely aggregated nanoparticulate ZnS.⁶ Some proteins strongly
60 bound to nanoparticles can decrease their size which is similar to the effects of
61 surfactants.⁷ Similarly, microbial extracellular polymeric substances (EPS), which
62 are composed of a variety of organic substances such as carbohydrates, proteins,
63 uronic acids and deoxyribonucleic acids, may either limit the dispersal or, in contrast,
64 stabilize the nanoparticles.⁸⁻¹⁰

65 Selenium nanoparticles (SeNPs) have been extensively used in a variety of
66 industries such as electronics and photonics. Biological methods have been explored
67 to synthesis SeNPs by reduction of selenium oxyanions, which is also considered to
68 be an effective bioremediation technique for selenium removal.¹¹⁻¹³ Recently, SeNPs
69 have been used for remediation of elemental mercury (Hg^0) contamination based on
70 the reaction: $Hg^0 + Se^0 \rightarrow HgSe$, because Se^0 is prone to reacting with Hg^0 to form
71 $HgSe$ (ΔG^0 of $-38.1 \text{ kJ mol}^{-1}$), the most stable inorganic mercury compound with a
72 K_{sp} of 1.0×10^{-59} .¹⁴⁻¹⁶ Normally, elemental mercury comprises only a small
73 proportion of the total mercury in soil whereas in mercury or gold mining regions
74 and in chlor-alkali plant soil, elemental mercury account for a huge part of the total
75 mercury¹⁷⁻¹⁹. Furthermore, dissolved elemental mercury is a significant mercury
76 species in natural waters, for instance, dissolved elemental mercury production

77 (~0.4-3.5% d⁻¹ of dissolved total mercury) was an important influence on the fate of
78 mercury in Long Island Sound.²⁰ The remediation efficiency of SeNPs for mercury
79 contaminated soil and water could be highly limited by their aggregation in the
80 complex soil solution or natural waters.

81 EPS is responsible for the colloidal properties of SeNPs, which govern the
82 fate of SeNPs in the environment and bioremediation performance.^{21,22} Therefore, it
83 is essential to investigate the effects of EPS on SeNPs under natural conditions and
84 the impact on mercury remediation using SeNPs.

85 In this study, the binding ability of EPS to SeNPs and resulting modification
86 of the SeNPs surface were examined by fluorescence excitation emission matrix
87 (EEM) spectroscopy, fluorescence quenching titration, Fourier transform infrared
88 spectroscopy (FTIR) and potentiometric titrations. Hydrodynamic diameter
89 distribution, zeta potential, and settling efficiency of SeNPs in the absence and
90 presence of EPS were measured to investigate effects of EPS on the stability of
91 SeNPs. Finally, the impacts of EPS on elemental mercury immobilization by SeNPs
92 were also investigated.

93

94 **Experimental**

95 **Extraction and characterization of EPS**

96 The SeNP producing bacterium *Citrobacter freundii* Y9, isolated from

97 anaerobic sulfate-reducing sludge, was cultivated at 30°C in a medium containing
98 1.0 g K₂HPO₄, 0.1 g MgCl₂, 0.2% yeast extract, 10 mM { [HYPERLINK](http://dict.cn/sodium%20citrate)
99 "<http://dict.cn/sodium%20citrate>" } in 1 L Milli-Q water (18 MΩcm⁻¹). To extract EPS, *C.*
100 *freundii* Y9 culture was firstly centrifuged (Anke GL-20G- II, Shanghai, China) at
101 3300 g × 10 min at 4°C. The harvested biomass was re-suspended in Milli-Q water
102 and centrifuged again at 16600 g for 20 min at 4°C. The supernatant was filtered
103 using 0.45 μm pore size membranes and then purified using a dialysis membrane
104 (3500 Da) at 4°C for 24 h.²³ Total organic carbon (TOC) content of EPS solution was
105 quantified by a TOC analyzer (TOC-4100, Shimadzu, Japan). The content of
106 polysaccharides and proteins was measured by the phenol-sulfuric acid method and
107 the Lowry method, respectively.^{24,25}

108 **Soil solution and ground water**

109 The effects of EPS on SeNPs was investigated in groundwater and soil
110 solution. Groundwater, taken from Urumqi, Xinjiang, China, was filtered through
111 0.45 μm membranes and then kept at 4°C. Soil solution was prepared according to
112 the following protocol. 10 g of soil taken from farmland was mixed with 50 ml Milli-
113 Q water and shaken for 18 h. The mixture was centrifuged for 20 min at 4400 g and
114 the supernatant filtered through 0.45 μm membranes.²⁶ After that the soil solution
115 was purified with a dialysis membrane (500 Da) at 4°C for 24 h in order to remove
116 dissolved organic matter. TOC of ground water and soil solution was measured as

117 described above. pH was measured using a Mettler Seven Easy pH meter (Mettler
118 Toledo, Greifensee, Switzerland), conductivity was determined with a DDSJ-308A
119 conductivity meter (REX Instrument Factory, Shanghai, China), Cl^- and SO_4^{2-} were
120 analyzed using a Dionex ICS 5000 ion chromatograph (Thermo Fisher Scientific,
121 Waltham, USA), CO_3^{2-} and HCO_3^- were analysed using a Mettler-Toledo G20
122 automatic titrator (Mettler Toledo, Greifensee, Switzerland), K^+ , Ca^{2+} , Na^+ , Mg^{2+}
123 were quantified by ICP-OES 735-ES (Agilent Technologies, Tokyo, Japan). The
124 physico-chemical properties of the soil solution included pH (7.99), conductivity
125 ($456 \mu\text{S cm}^{-1}$), TOC (11.38 mg L^{-1}), Cl^- (24.57 mg L^{-1}), SO_4^{2-} (95.79 mg L^{-1}), Ca^{2+}
126 (73.96 mg L^{-1}), K^+ (1.51 mg L^{-1}), Mg^{2+} (9.85 mg L^{-1}), Na^+ (34.56 mg L^{-1}), CO_3^{2-} (0
127 mg L^{-1}) and HCO_3^- (160.63 mg L^{-1}). The physico-chemical composition of
128 groundwater included pH (8.42), conductivity ($1153 \mu\text{S cm}^{-1}$), TOC (1.17 mg L^{-1}),
129 Cl^- (76.95 mg L^{-1}), SO_4^{2-} (352.49 mg L^{-1}), Ca^{2+} (6.74 mg L^{-1}), K^+ (20.22 mg L^{-1}),
130 Mg^{2+} (8.41 mg L^{-1}), Na^+ (254.80 mg L^{-1}), CO_3^{2-} (0 mg L^{-1}) and HCO_3^- (175.48 mg
131 L^{-1}).

132 **Preparation of SeNPs and EPS-capped CheSeNPs**

133 Chemically synthesized SeNPs (CheSeNPs) were synthesized by reduction of
134 sodium selenite with ascorbic acid. The produced SeNPs were purified according to
135 the following protocol.²⁷ The SeNPs supernatant was sonicated in a digital
136 ultrasonic bath (Hu20500B, Tianjin, China) followed by hexane separation and then

137 collected by centrifugation at 10000 g and 4°C for 10 min. After that **CheSeNPs** were
138 freeze-dried in a vacuum freeze dryer (Labconco, Kansas, USA). f

139 Biological SeNPs (BioSeNPs) were obtained by bioreduction of 1 mM
140 selenite by *C. freundii* Y9. Supernatants were collected by centrifugation at 10000 g
141 and 4°C for 10 min, and then purified as follows.²⁸ The precipitate was washed with
142 Tris-HCl (10 mM, pH 7.4) two times and re-suspended in 2% (w/v) sodium dodecyl
143 sulfate and 0.2 M NaOH. After that the precipitate was put in ultrasonic cell disruptor
144 (Scientz Biotechnology, Ningbo, China) at 120 W for 10 min in an ice bath, then
145 centrifuged (10000 g, 4°C, 10 min) and washed with Milli-Q water more than three
146 times. Finally, the precipitate was freeze-dried.

147 To obtain SeNPs capped by 20 and 100 mg L⁻¹ EPS, **CheSeNPs** were added
148 into 20 or 100 mg L⁻¹ EPS containing soil solution or groundwater and mixed at 200
149 rpm using a magnetic stirrer for 6 h (Jinyi Technology, Jintan, China) and sonicated
150 (Hengao Technology, Tianjin, China) for 5 min. Afterwards, the precipitate was
151 harvested by centrifugation at 10000 g and 4°C for 10 min and freeze-dried. The
152 concentration of **CheSeNPs** used was 100 mg L⁻¹ unless otherwise stated.

153 **Characterization of **CheSeNPs** and EPS-capped **CheSeNPs****

154 Hydrodynamic diameter distribution and zeta potential of **CheSeNPs** and
155 EPS-capped **CheSeNPs** were measured using a laser size distribution analyzer
156 (Zetasizer Nano ZS90, Malvern, Worcestershire, UK). For hydrodynamic diameter

157 distribution measurements, samples were prepared as follows. 1 mg sample was
158 added to 10 ml soil solution or groundwater and sonicated (Hengao Technology,
159 Tianjin, China) for 15 min and the hydrodynamic diameter distribution was
160 measured immediately. The zeta potential of SeNPs in the soil solution or
161 groundwater at different pH values was measured as follows. Soil solution or
162 groundwater pH was carefully adjusted using NaOH (0.1 M) and HCl (0.1 M) to pH
163 of 3, 5, 7, 9 or 11. Then 1 mg sample was added to 10 ml soil solution/groundwater
164 and the mixture sonicated for 30 min. EPS was used as a control for zeta potential
165 measurements. Zeta potential was calculated based on the Smoluchowski
166 approximation, and for each measurement, samples were first equilibrated for 120 s
167 and zeta-potential detection carried out in triplicate.

168 To determine pK_a and the surface charge of CheSeNPs and EPS-capped
169 CheSeNPs, potentiometric titration was carried out using a Metrohm 702 SM
170 potentiometric titrator (Metrohm Ltd., Herisau, Switzerland). 0.01 g sample was
171 dissolved in 50 ml background electrolyte (0.1 M NaNO₃). The initial pH of solution
172 was decreased to ~2 using 0.1 M HCl. The titration was conducted by automatic
173 addition of 0.02 ml aliquots of NaOH (0.1 M). For the control titration, 200 mg L⁻¹
174 EPS containing NaNO₃ (0.1 M) was performed separately.

175 FTIR spectroscopical analysis

176 For FTIR analysis, about 1 mg sample was ground with 100 mg KBr in an

177 agate mortar. FTIR spectra over the range 4000-400 cm^{-1} at a resolution of 4 cm^{-1}
178 were detected by a Bruker Vertex 70/V spectrometer (Bruker, Berlin, Germany)
179 equipped with a D-LaTGS-detector. All samples were scanned three times to
180 determine the changes in vibration frequency of the functional groups, with no
181 significant difference between the spectra. The background obtained from the
182 **scanning** of pure KBr was automatically subtracted from the sample spectra.

183 **Fluorescence spectroscopy and quenching titration**

184 3D excitation and emission **fluorescence** spectroscopy of EPS was obtained
185 using a Hitachi F-7000 fluorescence spectrophotometer (Hitachi, Tokyo, Japan)
186 equipped with a 1.0 cm quartz cell and a thermostatic bath. The EEM spectra were
187 collected at 5 nm increments over an excitation range of 200-500 nm, with an
188 emission range of 200-500 nm every 2 nm with an excitation/emission slit of 5.0 nm.
189 The scanning speed was 1200 nm min^{-1} . Milli-Q water was set as the blank which
190 was subtracted from the sample EEM spectra. EEM spectral images were generated
191 using SigmaPlot 10.0 (Systat, US). EPS solutions were titrated with incremental μL
192 addition of 4.22 mM **CheSeNPs** suspension at 298 K. After each addition of SeNPs
193 solution, the solution was fully mixed using a magnetic stirrer for 15 min and the
194 fluorescence spectra recorded. The equilibrium time was set as 15 min since
195 fluorescence intensities at peaks varied little after 15 min reaction time.

196 **Settling experiments**

197 The settling experiments for 100 mg L⁻¹ of **CheSeNPs**/EPS-capped
198 **CheSeNPs** were conducted in soil solution, groundwater and Milli-Q water. The
199 suspensions were homogenized in an ultrasonic bath (Hu20500B, Tianjin, China)
200 at 35 kHz and 240 W for 20 min. OD_{600nm} was measured 3 cm below the liquid
201 surface using a Cary 60 UV-Vis spectrophotometer (Agilent Technology, Santa
202 Clara, USA), which represents the concentration of SeNPs.

203 **Impact of EPS on mercury remediation using SeNPs**

204 The impact of EPS on mercury immobilization using SeNPs was conducted
205 in Hg⁰ contaminated groundwater (Fig. S1). Hg⁰ contaminated ground water was
206 prepared according to a previous study as follows.²⁹ A small droplet of elemental Hg
207 was added into ground water which had already been purged for 30 min in a
208 sonicator (Hengao Technology, Tianjin, China). After that, the solution was
209 sonicated for another 30 min and then stabilized overnight:the supernatant was
210 collected as Hg⁰ contaminated groundwater. The Hg⁰ solution was used within 2 h
211 to avoid oxidation. **100 ml Hg⁰ contaminated groundwater/soil solution containing**
212 **50 mg L⁻¹ SeNPs in the presence of 0, 1, 10, 50, 100, 200 mg L⁻¹ of EPS were added**
213 **into a 500 ml jar. CheSeNPs** and BioSeNPs were both used in the present study. The
214 sealed jar was shaken at 130 rpm in an incubator shaker (Crystal IS-RSV3, Dallas,
215 USA) overnight, and after that the Hg⁰ concentration was measured using a mercury
216 analyzer (Lumex RA915+, Saint Petersburg, Russia). For mercury analysis, the high

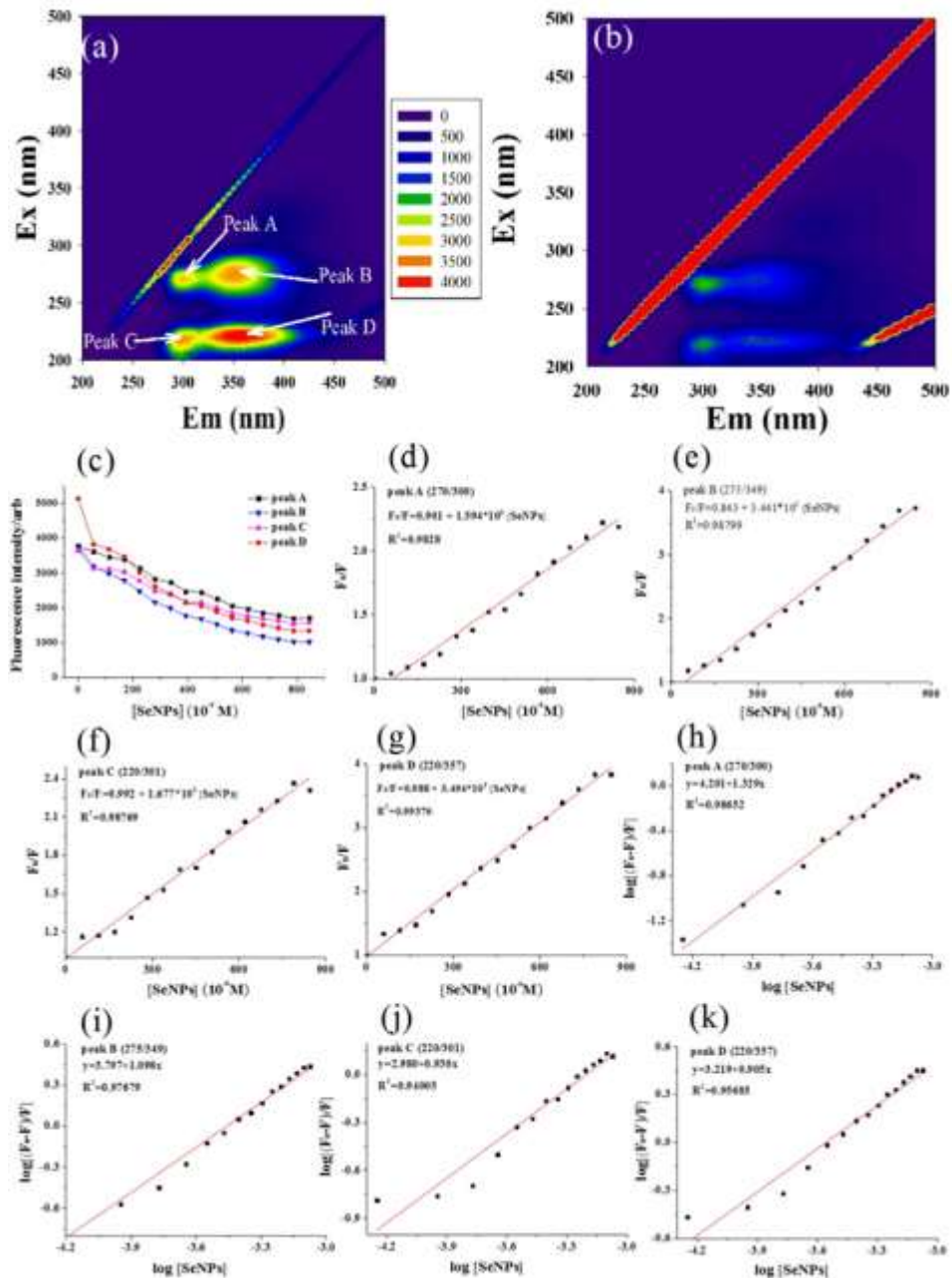
217 concentration mode was selected and an additional cell for analysis was used. The
218 sample flow rate was set 1.0 L min^{-1} , and KMnO_4 solution (5%) was used to capture
219 mercury-containing waste gas. A control without the supply of SeNPs and EPS was
220 also conducted.

221 All the experiments were conducted in triplicate and mean values were used.

222

223 **Results**

224 **Fluorescence quenching titration of EPS with **CheSeNPs****



225

226 Fig. 1. (a) Typical three-dimensional fluorescence EEM spectrum of EPS; (b) three-
 227 dimensional fluorescence EEM spectrum of EPS after addition of 4.22 mM
 228 **CheSeNPs**; (c) fluorescence quenching curves of EPS titrated with **CheSeNPs**
 229 solution. Values represent means \pm standard deviation of three independent

230 measurements. Bars indicate standard errors. (d) (e) (f) (g) are the Stern-Volmer plots
231 of fluorescence quenching of the peaks A, B, C and D of EPS titrated with **CheSeNPs**
232 solution. (h) (i) (j) (k) are the plots of $\log [(F_0-F)/F]$ versus $\log [\text{SeNPs}]$ of
233 fluorescence quenching of the peaks A, B, C and D of EPS titrated with **CheSeNPs**
234 suspension.

235
236 The EPS solution had a TOC content of 163.0 mg L^{-1} , with 19.1 mg L^{-1}
237 polysaccharide and 87.3 mg L^{-1} protein. The EEM fluorescence spectrum of EPS
238 showed the presence of four distinct peaks (Fig. 1a). The four peaks were designated
239 peaks A (Ex/Em=270/300), B (Ex/Em=275/349), C (Ex/Em=220/301) and D
240 (Ex/Em=220/357). The fluorescence intensity of these peaks significantly decreased
241 with the incremental addition of **CheSeNPs** (Fig. 1b, c), indicating strong binding of
242 EPS to the **CheSeNPs**. In order to obtain the binding parameters, the fluorescence
243 quenching data were further fitted to the Stern-Volmer equation (1) and the Hill
244 equation (2).^{30,31}

$$245 \quad F_0/F = 1 + k_q \tau_0 [\text{CheSeNPs}] = 1 + K_{SV}[\text{CheSeNPs}] \quad (1)$$

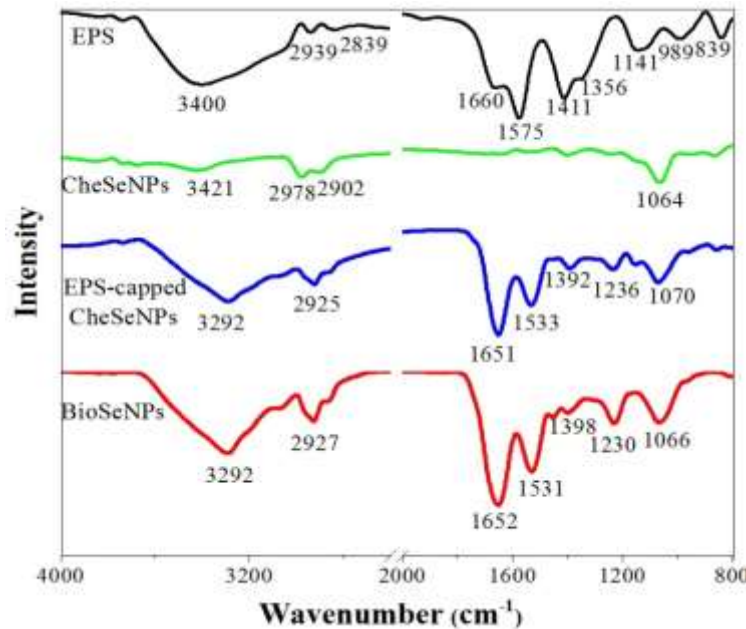
246 where F_0 and F are the fluorescence intensities in the absence or presence of
247 quencher; K_q = quenching rate constant; K_{sv} = quenching constant; τ_0 = average
248 lifetime of the fluorescence in the absence of quencher which is usually taken as 10^{-8}
249 s and $[\text{CheSeNPs}]$ = concentration of **CheSeNPs**. The fluorescence quenching

250 data well fitted to the Stern-Volmer equation (Fig. 6d, e, f, g). K_{sv} ($\times 10^3$ L mol⁻¹)
251 estimated from the Stern-Volmer equation for peaks A, B, C and D were was 1.59
252 ($R^2=0.98$), 3.44 ($R^2=0.99$), 1.68 ($R^2=0.99$) and 3.49 ($R^2=0.99$), respectively. The
253 calculated K_q ($\times 10^{11}$ L mol⁻¹ sec⁻¹) was as follows: 1.59, 3.44, 1.68, and 3.49.

254 Fluorescence intensity data were also used to estimate the binding constant
255 (K_b) and the number of binding sites (n) for binding of EPS to CheSeNPs using the
256 Hill equation (2):

$$257 \quad \log [(F_0-F)/F] = \log K_b + n \log [\text{CheSeNPs}] \quad (2)$$

258 where (F_0-F) = fraction of quenched fluorescence with CheSeNPs binding; K_b = a
259 binding constant that reflects the interactive intensity between the fluorophore and a
260 quencher; n = equivalent binding sites provided by fluorophore to the quencher
261 molecule. A good linear relationship was obtained between $\log [(F_0-F)/F]$ and \log
262 $[\text{CheSeNPs}]$ (Fig. 6h, i, j, k). The binding constant (K_b , $\times 10^3$ L mol⁻¹) for peaks A,
263 B, C and D were 15.9, 6.3, 0.95 and 1.7 respectively and n for peaks A, B, C and D
264 were 1.33, 1.10, 0.93 and 0.91, respectively.

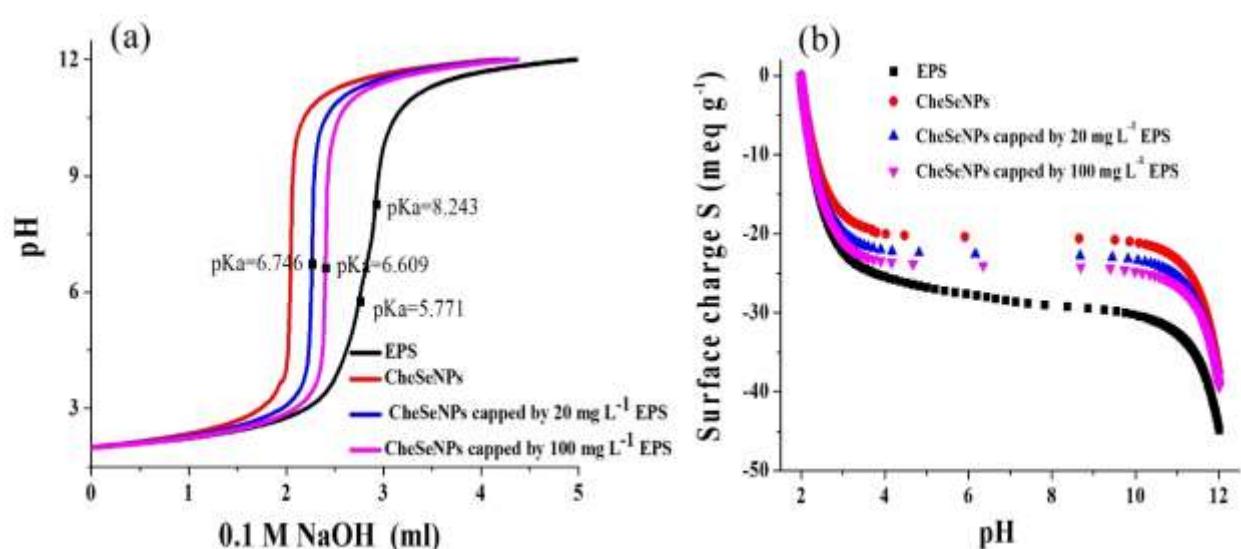


265
 266 Fig. 2. FTIR spectra of EPS, BioSeNPs, CheSeNPs and EPS-capped CheSeNPs.
 267 Typical results are shown from one of several determinations.

268 **FTIR spectroscopical analysis**

269 The FTIR spectrum of the EPS (Fig. 2) showed a broad –OH stretch peak at
 270 3400 cm⁻¹ and lipid –CH– vibration peaks at 2939 cm⁻¹ and 2839 cm⁻¹.^{32,33} The peak
 271 at 1660 cm⁻¹ confirms the presence of the carbonyl stretch of the amide I group and
 272 the peak at 1575 cm⁻¹ shows the combination of N-H bending and C-N stretching of
 273 amide II functionalities.^{34,35} The peak band appearing at 1411 cm⁻¹ is attributed to
 274 the symmetric stretching of the carboxylic group.³⁶ The 1356 cm⁻¹ peak indicates the
 275 adsorption band of C–H vibrations in the methyl group.³⁷ The peak at 1141 cm⁻¹
 276 corresponds to polysaccharide groups and the peak at 839 cm⁻¹ can be designated as
 277 glycosidic linkage bonds.^{35,38} The other minor absorption peaks ranging between

278 695-515 cm^{-1} are due to the stretching of alkyl-halides, and the other bands in the
 279 fingerprint zone ($<1000 \text{ cm}^{-1}$) might be attributed to phosphate groups.^{39,40} After
 280 adsorption of EPS, peaks at 1651, 1533, 1392 and 1236 cm^{-1} were observed in the
 281 FTIR spectrum of the **EPS-capped CheSeNPs**, indicating that the proteins,
 282 polysaccharides and lipids in the EPS were adsorbed to the **CheSeNPs** surface. **The**
 283 **FTIR pattern of the EPS-capped CheSeNPs was similar to that of the BioSeNPs.**

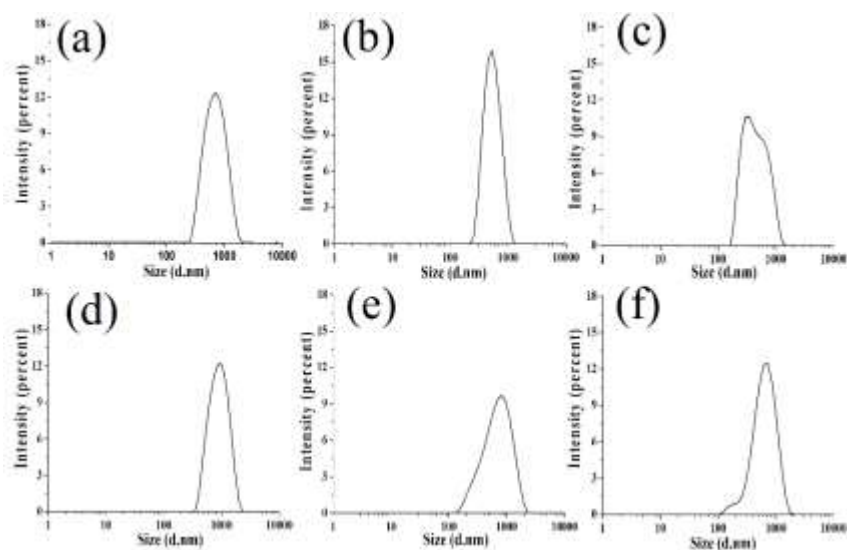


284
 285 Fig. 3. (a) Acid-base titration curves of **CheSeNPs**, EPS-capped **CheSeNPs** and EPS,
 286 and (b) potentiometric titration curves of **CheSeNPs**, EPS-capped **CheSeNPs** and
 287 EPS. Surface charge was calculated according to the data from acid-base titrations.
 288 Typical patterns are shown from one of two determinations both of which gave
 289 similar results.

290 **Potentiometric titrations and Surface charge**

291 The acid-base titration curves for EPS showed a smooth increase of pH with

292 increasing amounts of NaOH (Fig. 3a). The buffering capacity followed an order of
 293 EPS >100 mg L⁻¹ EPS capped **CheSeNPs** > 20 mg L⁻¹ EPS capped **CheSeNPs** >
 294 **CheSeNPs**. The acid-base titration data of EPS showed the presence of two major
 295 functional groups with pK_a values of 5.7 and 8.2. However, the pK_a was 6.75 for 20
 296 mg L⁻¹ EPS treated **CheSeNPs** and 6.61 for 100 mg L⁻¹ EPS treated **CheSeNPs**. It is
 297 seen from Fig. 3b that the surface charge became more negative with the increase of
 298 pH. The negative charge increased significantly between pH 2 and 4 because of the
 299 consumption of H⁺ ions, and then leveled off until the pH increased up to 10 with
 300 the surplus supply of OH⁻. The magnitude of surface charge number increased in the
 301 order of **CheSeNPs** < **CheSeNPs** capped by 20 mg L⁻¹ EPS < **CheSeNPs** capped
 302 by 100 mg L⁻¹ EPS < EPS.



303
 304 Fig. 4. Typical hydrodynamic diameter distribution curves of **CheSeNPs** (a),
 305 **CheSeNPs** capped by 20 mg L⁻¹ EPS (b) and **CheSeNPs** capped by 100 mg L⁻¹ EPS

306 (c) in ground water. Typical hydrodynamic diameter distribution curves of
307 **CheSeNPs** (d), **CheSeNPs** capped by 20 mg L⁻¹ EPS (e) and **CheSeNPs** capped by
308 100 mg L⁻¹ EPS (f) in soil solution. Typical curves are shown from one of several
309 determinations.

310

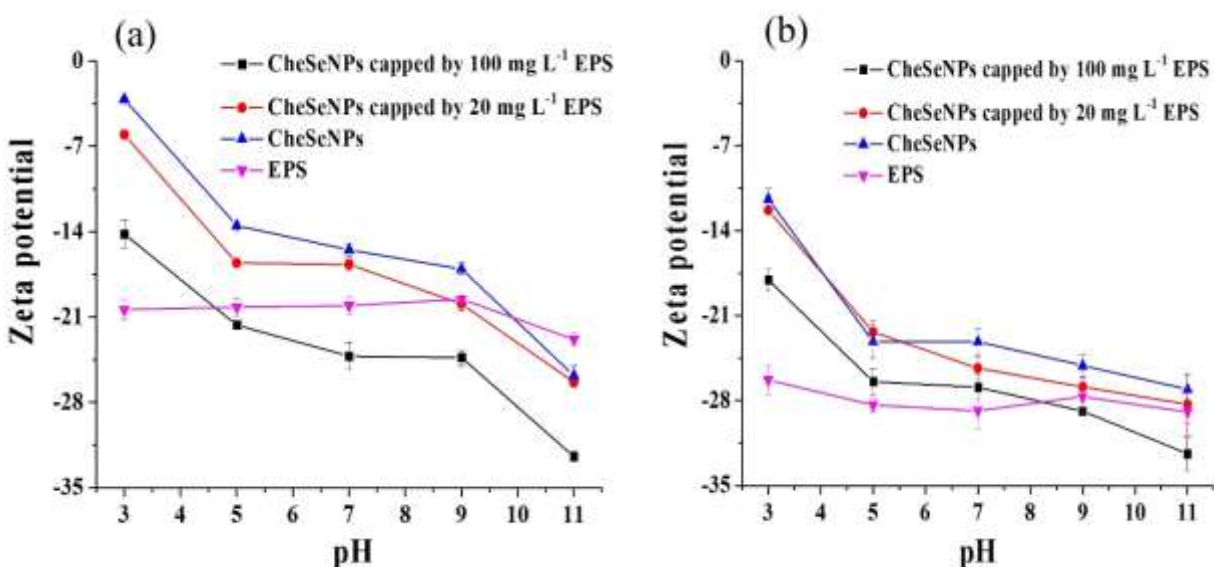
311 **Hydrodynamic diameter of SeNPs**

312 It is noted that the addition of EPS significantly changed the size distribution
313 pattern of **CheSeNPs** (Fig. 4). The average diameter of **CheSeNPs** in groundwater
314 was 740.2 nm, while in the presence of 20 and 100 mg L⁻¹ EPS, the average diameter
315 of **CheSeNPs** decreased to 556.9 and 484.3 nm, respectively. Similarly an average
316 diameter of **CheSeNPs** in soil solution was found to be 948.4 nm. However, the
317 addition of 20 and 100 mg L⁻¹ EPS solution decreased the average diameter of
318 **CheSeNPs** to 770.7 and 677.9 nm, respectively.

319 **Zeta potential of SeNPs**

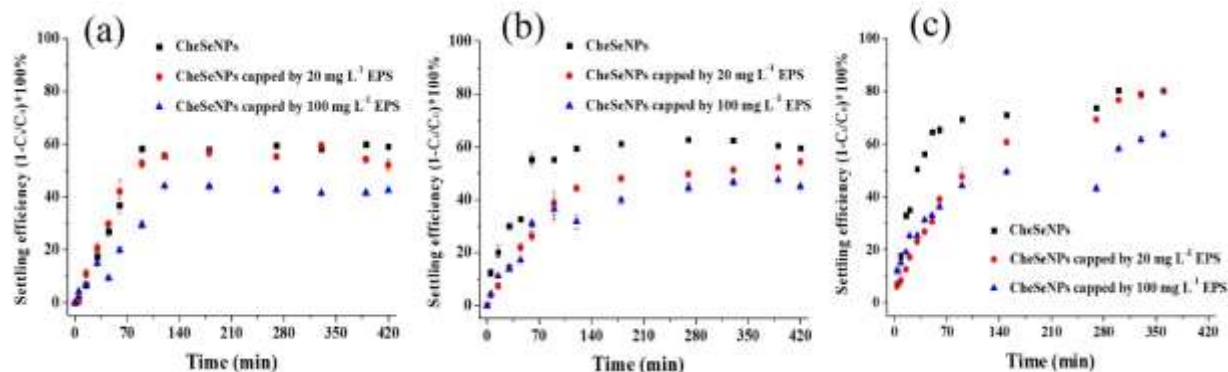
320 The zeta potential as a function of pH for **CheSeNPs**, EPS-capped **CheSeNPs**
321 and EPS in soil solution/groundwater are shown in Fig. 5. It can be noted that the
322 zeta potential of EPS slightly changed over the pH range from pH 3 to 11 in both
323 groundwater and soil solution respectively. The average zeta value was -20.61 ± 1.29
324 and -28.02 ± 0.08 for EPS in groundwater and soil solution, respectively. These
325 values demonstrated that EPS suspension was colloidally stable. The zeta potential

326 of **CheSeNPs** significantly decreased when the pH increased from 3 to 11. However,
 327 in the presence of EPS, the zeta potential of EPS-capped **CheSeNPs** became more
 328 negative than **CheSeNPs** and this phenomenon was more predominant in
 329 groundwater compared to the soil solution. In groundwater, the magnitude of zeta
 330 potential was in the order **CheSeNPs** < **CheSeNPs** capped by 20 mg L⁻¹ EPS < EPS
 331 < **CheSeNPs** capped by 100 mg L⁻¹ EPS between pH 5 and 9. In the soil solution,
 332 the zeta potential of **CheSeNPs** capped by 100 mg L⁻¹ EPS was similar to EPS, which
 333 was higher than **CheSeNPs** capped by 20 mg L⁻¹ EPS and **CheSeNPs**.



334
 335 Fig. 5. (a) Zeta potential as a function of pH for **CheSeNPs**, EPS-capped **CheSeNPs**
 336 and EPS in the ground water; and (b) Zeta potential as a function of pH for
 337 **CheSeNPs**, EPS-capped **CheSeNPs** and EPS in the soil solution. Values represent
 338 the mean values of three independent measurements. Bars indicate standard errors.

339



340
 341 Fig. 6. Settling experiment of **CheSeNPs** and EPS-capped **CheSeNPs** in (a)
 342 groundwater, (b) soil solution, and (c) Milli-Q water. C_i is the concentration of
 343 SeNPs detected over time, C_0 is the initial concentration of SeNPs. The
 344 concentration of SeNPs was indicated by OD_{260nm} of the suspension. Error bars
 345 represent the standard deviation ($n=3$).

346
 347 **Settling efficiency**

348 In groundwater, a slight difference of the settling efficiency between
 349 **CheSeNPs** capped by 20 mg L^{-1} EPS (55.56%) and **CheSeNPs** (58.85%) was
 350 observed (Fig. 6a). However, this decreased to 42.78% for **CheSeNPs** capped by 100
 351 mg L^{-1} EPS. In soil extract, the settling efficiency significantly decreased with
 352 increasing concentration of EPS (Fig. 6b). It was noted that that 60.93% of
 353 **CheSeNPs** settled within 2 h in the absence of EPS while the presence of 20 and 100
 354 mg L^{-1} EPS slowed the settling process down to 51.83% and 45.89% respectively
 355 over 6 h. Similar settling experiments for **CheSeNPs** were performed in Milli-Q

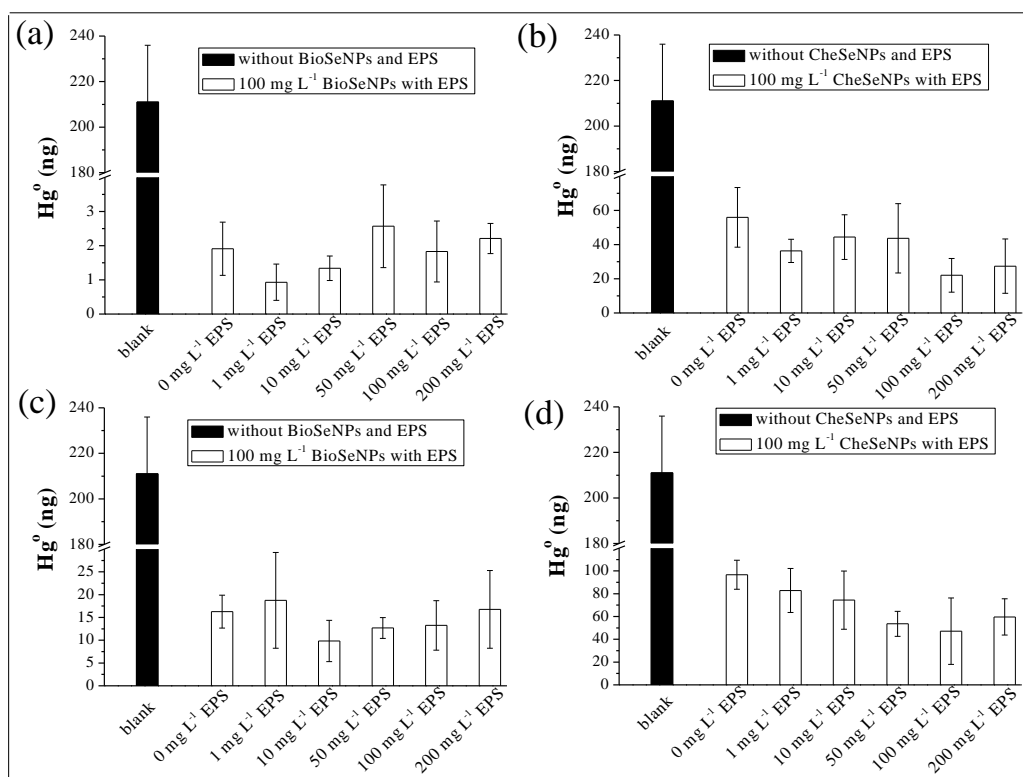
356 water as controls. It is seen in Fig. 3c that **CheSeNPs** readily settled in 2 h with a
357 settling efficiency of 79.78% which was similar to the settling efficiency of
358 **CheSeNPs** capped by 20 mg L⁻¹ EPS over 6 h. However, the settling efficiency
359 decreased to 61.27% for **CheSeNPs** capped by 100 mg L⁻¹ EPS.

360 **Impact of EPS on mercury remediation using SeNPs**

361 The remediation efficiency of Hg⁰ contaminated groundwater and soil
362 solution by BioSeNPs or CheSeNPs in the absence and presence of EPS are shown
363 in Fig. 7. In the case of groundwater, addition of 100 mg L⁻¹ BioSeNPs significantly
364 reduced the Hg⁰ content from an initial 211 ng to 1.9 ng with a 99.1% removal
365 efficiency. The influence of EPS on Hg⁰ remediation by BioSeNPs was not
366 significant. Addition of 1 mg L⁻¹ EPS slightly enhanced Hg⁰ removal. However
367 higher concentrations of EPS showed little inhibition of Hg⁰ removal efficiency. The
368 CheSeNPs showed a much lower removal efficiency, 73.5%, for Hg⁰ in comparison
369 with the BioSeNPs. Addition of 1-200 mg L⁻¹ EPS generally increased Hg⁰ removal.
370 Addition of 1 and 100 mg L⁻¹ EPS resulted in increases in the Hg⁰ removal
371 percentage to 82.7% and 85.9%, respectively. The effect of EPS on Hg⁰ removal in
372 the soil solution by BioSeNPs and CheSeNPs was similar to that in the groundwater.
373 However, much higher concentrations of EPS were required for improving Hg⁰
374 removal from the soil solution than from the groundwater. 10 and 100 mg L⁻¹ EPS
375 were the optimal dosages for Hg⁰ removal from the soil solution by BioSeNPs and

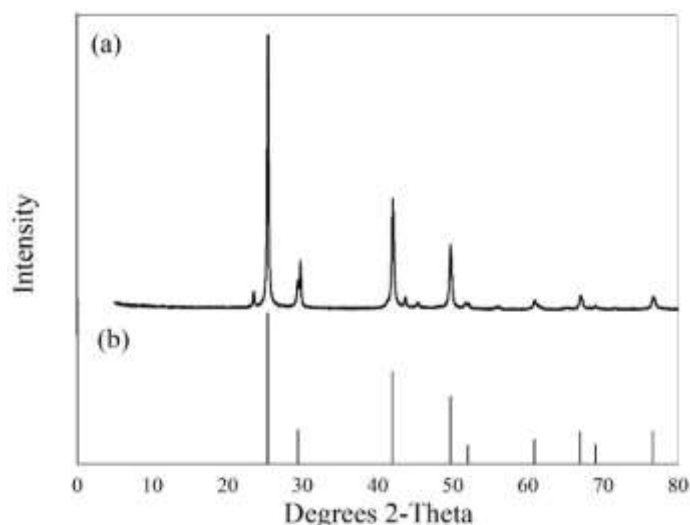
376 CheSeNPs, respectively. The possible reason for this may be the more complex
 377 composition of the soil solution than the groundwater.

378 It is found that most of the Hg^0 (over 88.8%) was removed as a precipitate
 379 from the groundwater and the soil solution by BioSeNPs and CheSeNPs in the
 380 absence and presence of EPS (Table 1). XRD analysis confirmed Hg in the
 381 precipitate was predominantly $HgSe$, which is the product of interaction between Se^0
 382 and Hg^0 (Fig. 8).



383
 384 Fig. 7. The effect of EPS on Hg^0 immobilization from groundwater using (a)
 385 BioSeNPs and (b) CheSeNPs; the effects of EPS on Hg^0 remediation of the soil
 386 solution using (c) BioSeNPs and (d) CheSeNPs. The blank is the Hg^0 contaminated

387 groundwater or soil solution without addition of SeNPs and EPS. Error bars (n=3)
 388 represent the standard deviation.



389
 390 Fig. 8. XRD pattern of the precipitate collected from CheSeNPs treated Hg⁰
 391 containing ground water. A typical pattern is shown from one of several
 392 determinations.

393 Table 1. Total amount of Hg removed from groundwater or soil solution, the amount
 394 of Hg in the precipitate, and the proportions of precipitated Hg among the total Hg
 395 removed from groundwater or soil solution. All the data are the averages of three
 396 replicated measurements. The data are presented as average ± standard deviation.

Treatment	Total Hg removed from groundwater (ng)	Hg in the precipitate (ng)	Proportion of precipitated Hg (%)
Groundwater BioSeNPs + 0 mg L ⁻¹ EPS	209.1 ± 36.4	198.5 ± 2.8	94.9

	BioSeNPs + 1 mg L ⁻¹ EPS	210.1 ± 36.0	204.3 ± 7.4	97.3%
	BioSeNPs + 10 mg L ⁻¹ EPS	209.7 ± 35.8	207.5 ± 13.4	98.9%
	BioSeNPs + 50 mg L ⁻¹ EPS	208.4 ± 36.9	194.6 ± 10.2	93.4%
	BioSeNPs + 100 mg L ⁻¹ EPS	209.2 ± 36.5	188.2 ± 16.2	89.9%
	BioSeNPs + 200 mg L ⁻¹ EPS	208.8 ± 35.8	211.7 ± 6.1	101.4%
	CheSeNPs + 0 mg L ⁻¹ EPS	155.1 ± 59.9	142.7 ± 8.1	92.0%
	CheSeNPs + 1 mg L ⁻¹ EPS	174.7 ± 44.9	176.39 ± 10.4	100.9%
	CheSeNPs + 10 mg L ⁻¹ EPS	166.6 ± 53.7	160.2 ± 19.2	96.1%
	CheSeNPs + 50 mg L ⁻¹ EPS	167.3 ± 63.9	180.5 ± 23.6	107.9%
	CheSeNPs + 100 mg L ⁻¹ EPS	188.9 ± 49.2	203.6 ± 12.6	107.7%
	CheSeNPs + 200 mg L ⁻¹ EPS	183.6 ± 57.8	190.7 ± 3.5	103.8%
Soil solution	BioSeNPs + 0 mg L ⁻¹ EPS	194.7 ± 40.4	172.9 ± 13.1	88.8%
	BioSeNPs + 1 mg L ⁻¹ EPS	192.3 ± 50.1	200.1 ± 10.4	104.1%
	BioSeNPs + 10 mg L ⁻¹ EPS	201.2 ± 41.7	187.8 ± 23.6	93.3%
	BioSeNPs + 50 mg L ⁻¹ EPS	198.3 ± 38.5	174.3 ± 11.9	87.9%
	BioSeNPs + 100 mg L ⁻¹ EPS	197.8 ± 42.9	190.2 ± 19.3	96.2%
	BioSeNPs + 200 mg L ⁻¹ EPS	194.2 ± 47.3	206.4 ± 20.5	106.3%
	CheSeNPs + 0 mg L ⁻¹ EPS	114.4 ± 53.2	123.8 ± 22.4	108.2%
	CheSeNPs + 1 mg L ⁻¹ EPS	128.2 ± 62.5	140.6 ± 17.5	109.7%

CheSeNPs + 10 mg L ⁻¹ EPS	136.6 ± 71.3	130.7 ± 27.1	95.7%
CheSeNPs + 50 mg L ⁻¹ EPS	157.4 ± 50.7	170.8 ± 33.5	108.5%
CheSeNPs + 100 mg L ⁻¹ EPS	163.9 ± 76.5	158.2 ± 25.3	96.5%
CheSeNPs + 200 mg L ⁻¹ EPS	151.4 ± 57.8	140.9 ± 33.7	93.1%

397

398

399 Discussion

400 This study shows that there was a strong interaction between the SeNPs and
401 the EPS from a selenite-reducing bacterium and this strong binding of EPS to NPs
402 improved the stability of NPs. Nanoparticles tend to bind with EPS.⁴¹ The
403 fluorescence quenching titration data (Fig. 1) confirmed that the fluorescent
404 components, including the tyrosine-like (peak A), the tryptophan-like substances
405 (peak B), the protein-like substances (aromatic I proteins) (peak C) and the protein-
406 like substances (aromatic II proteins) (peak D) have a strong binding ability to the
407 SeNPs.^{42,43} The quenching constant (K_q , $\times 10^{11}$ L mol⁻¹ sec⁻¹) (1.59-3.49) for EPS and
408 CheSeNPs was one order of magnitude bigger than the maximum diffusion collision
409 quenching rate constant (2.0×10^{10} mol⁻¹ sec⁻¹), implying that the fluorescence
410 quenching process was mainly governed by static quenching which is usually
411 induced by complexation between the fluorophore and the quencher molecules. The
412 binding constant (K_b , $\times 10^3$ L mol⁻¹) for the complexation of EPS with
413 CheSeNPs, calculated according to the Hill equation, was found to range from 0.95

414 to 15.9, which is close to the values reported for the binding of toxic metals to EPS.⁴⁴
415 It can be concluded that the binding ability between EPS and CheSeNPs was similar
416 to those between EPS and toxic metals. The binding site number (n) for the EPS-
417 CheSeNPs complexes was close to 1 (0.91-1.33), which indicated that there was only
418 one independent class of binding site present in the EPS that participated in trapping
419 CheSeNPs. It can be concluded that the binding of CheSeNPs to EPS was mainly
420 governed by the proteins in the EPS. The FTIR spectra revealed that proteins,
421 carboxylates, polysaccharides and lipids were adsorbed onto CheSeNPs (Fig. 2). The
422 acid-base potentiometric titration curves (Fig. 3) further confirmed binding of
423 proteins, carboxyl and amine groups onto CheSeNPs.^{45,46} Adsorption of these
424 functional groups increased the buffering capacity of EPS-capped CheSeNPs.

425 In order to examine the stabilizing effect of EPS on SeNPs, CheSeNPs were
426 used instead of BioSeNPs, because the surface of BioSeNPs are already covered
427 with EPS.^{27,47} The zeta potential, hydrodynamic diameter and attachment efficiency
428 data show that EPS from the selenite-reducing bacterium acted as an excellent
429 natural dispersant that can stabilize SeNPs in soil solution or groundwater by
430 inhibition of aggregation (Fig. 4, 5, 6). EPS in the soil solution and groundwater
431 have zeta potential values of about -21 mv and -28 mv, respectively. Adsorption of
432 more negative EPS molecules significantly made SeNPs more negatively charged
433 (Fig. 5). EPS can provide colloidal stability to nanoparticles either by electrostatic,

434 steric or electrosteric mechanisms.^{48,49} In the present study, EPS-capped **CheSeNPs**
435 were more negatively charged compared to **CheSeNPs** and this increased the
436 electrostatic force of repulsion between particles and increased the stability of
437 SeNPs.⁵⁰ EPS therefore plays an important role in controlling the surface charge of
438 BioSeNPs which will govern the fate of selenium nanoparticles.^{22,27} A similar role
439 of EPS on the stability of silver nanoparticles has been documented.⁵⁰ However, the
440 effects of EPS on stability of nanoparticles reported in the literature are contradictory.
441 It was found that EPS destabilizes Ag nanoparticles and promotes their aggregation
442 to protect cells.⁵¹ Polysaccharides can also destabilize colloidal particles.⁴⁵ The
443 contradictory stabilizing or destabilizing effects of EPS may be relevant to different
444 composition of EPS from different sources. More work is needed to understand the
445 key components that affect the stability of NPs.

446 Addition of EPS increases stability of SeNPs, associated with the decrease in
447 hydrodynamic diameter, and decreased their settling efficiency (Fig. 6). The
448 stabilizing effect of EPS therefore improves remediation of Hg⁰ contaminated soil
449 solution and groundwater by CheSeNPs (Fig. 7). **For the BioSeNPs treatment group,**
450 it was found that when the EPS dosage increased from 1 to 200 mg L⁻¹, the
451 remediation efficiency was not significantly increased. Although EPS improves the
452 remediation performance, BioSeNPs were more efficient for Hg⁰ removal than
453 CheSeNPs. This may be explained because BioSeNPs are covered by EPS during

454 their synthesis.⁵² The EPS bound to the surface of BioSeNPs is helpful for the
455 stability of SeNPs compared with CheSeNPs, and agglomeration of CheSeNPs
456 significantly inhibited the efficiency of mercury remediation. Similarly, 1 mg L⁻¹
457 EPS significantly enhanced remediation performance by BioSeNPs but a higher
458 dosage of EPS inhibited Hg⁰ removal by BioSeNPs. It is likely that too much EPS
459 blocked Hg⁰ access to the SeNPs surfaces or chemically passivated the surface
460 through Se-thiol reactions. The immobilization of Hg⁰ using SeNPs occurs by
461 adsorption or a gas-solid reaction where performance highly depends on surface area.
462 Hg⁰ capture using bovine serum albumin (BSA) stabilized SeNPs was hindered in
463 comparison with SeNPs synthesized without BSA, despite a huge increase in the
464 available surface area. This was attributed to surface passivation by BSA which
465 decreased the density of available reactive sites on the surface of SeNPs.⁵² Similarly,
466 the bacterially derived organic substances bound to the surface of SeNPs increased
467 the stability of SeNPs but too much organic substances may passivate the surface
468 and thus reduce Hg⁰ removal efficiency.^{53,54} These studies are in good agreement
469 with our present study. Generally, a low dosage of EPS (e.g., 1 mg L⁻¹) is most cost-
470 effective for enhancing remediation of Hg⁰ contaminated soil and water by
471 Bio/CheSeNPs from the perspective of an engineering application.

472 **Conclusions**

473 *C. freundii* Y9 EPS can significantly reduce aggregation and improve the

474 stability of SeNPs in soil solution and groundwater because of adsorption to SeNPs
475 forming more negatively charged SeNPs. EPS can enhance the remediation
476 efficiency of soil solution and groundwater contaminated with Hg⁰ using SeNPs. A
477 lower dosage of EPS is most cost-effective for Hg⁰ remediation of groundwater and
478 a higher dosage is required for remediation of soil solution. This study highlights
479 that the EPS of *C. freundii* Y9 is an excellent natural dispersant of SeNPs and can be
480 used as effective amendment for improving mercury immobilization by SeNPs.

481 **Acknowledgments**

482 This work was supported by the National Natural Science Foundation of China
483 (U1503281 and U1403181). G. M. Gadd also gratefully acknowledges an award
484 (NE/M01090/1) under the National Environmental Research Council (UK) Security
485 of Supply of Mineral Resources Grant Program: Tellurium and Selenium Cycling
486 and Supply (TeASe).

487 **Conflict of Interest Disclosure**

488 The authors declare no competing financial interest.

489

490 **References**

- 491 **1.** J. Lahann, *Nat. Nanotechnol.*, 2008, **3**, 320-321.
- 492 **2.** Y. Sun, X. Li, W. Zhang and H. Wang, *Colloids Surf. A Physicochem. Eng. Asp.*,
493 2007, **308**, 60-66.

- 494 3. B. Schrick, B. W. Hydutsky, J. L. Blough and T. E. Mallouk, *Chem. Mater.*, 2004,
495 **16**, 2187-2193.
- 496 4. F. He, and D. Zhao, *Environ. Sci. Technol.*, 2005, **39**, 3314-3320.
- 497 5. R. Kretzschmar, and H. Sticher, *Environ. Sci. Technol.*, 1997, **31**, 3497-3504.
- 498 6. J. W. Moreau, R. I. Webb, and J. F. Banfield, *Am. Mineral.*, 2004, **89**, 950-960.
- 499 7. J. Dobias, E. I. Suvorova, and R. Bernier-Latmani, *Nanotechnology*, 2011, **22**,
500 195605.
- 501 8. B. Frølund, R. Palmgren, K. Keiding, and P. H. Nielsen, *Water Res.*, 1996, **30**,
502 1749-1758.
- 503 9. J. W. Moreau, P. K. Weber, M. C. Martin, B. Gilbert, I. D. Hutcheon, and J. F.
504 Banfield, *Science*, 2007, **316**, 1600-1603.
- 505 10.C. Zhou, Z. Wang, A. Marcus and B. E. Rittmann, *Environ. Sci.: Nano*, 2016, **3**,
506 1396-1404.
- 507 11.S. L. Hockin, and G. M. Gadd, *Appl. Environ. Microbiol.*, 2003, **69**, 7063-7072.
- 508 12.S. Hockin, and G. M. Gadd, *Environ. Microbiol.*, 2006, **8**, 816-826.
- 509 13.X. Xia, L. Ling and W. Zhang, *Environ. Sci.: Nano*, 2016, **4**, 52-59.
- 510 14.N. Ralston, *Nat. Nanotechnol.*, 2008, **3**, 527-528.
- 511 15.J. Fellowes, R. Patrick, D. Green, A. Dent, J. Lloyd, and C. Pearce, *J. Hazard.*
512 *Mater.*, 2011, **189**, 660-669.
- 513 16.X. Wang, D. Zhang, X. Pan, D. J. Lee, F. A. Al-Misned, M. G. Mortuza, and G.

- 514 M. Gadd, *Chemosphere*, 2017, **170**, 266-273.
- 515 17.D. Kocman, M. Horvat, and J. Kotnik, *J. Environ. Monit.*, 2004, **6**, 696-703.
- 516 18.A. García-Sánchez, F. Contreras, M. Adams, and F.Santos, *Environ. Geochem.*
517 *Health*, 2006, **28**, 529-540.
- 518 19.C. M. Neculita, G. J. Zagury, and L. Deschenes, *J. Environ. Qual.*, 2005, **34**, 255-
519 262.
- 520 20.K. R. Rolfhus, and W. F. Fitzgerald, *Geochim. Cosmochim. Acta*, 2001, **65**, 407-
521 418.
- 522 21.Y. Zhang, Z. A. Zahir, and W. T. Frankenberger, *J. Environ. Qual.*, 2004, **33**, 559-
523 564.
- 524 22.B. Buchs, M. W. Evangelou, L. H. Winkel, and M. Lenz, *Environ. Sci. Technol.*,
525 2013, **47**, 2401-2407.
- 526 23.S. S. Aday, and D. J. Lee, *J. Hazard. Mater.*, 2008, **154**, 1120-1126.
- 527 24.M. Dubois, K. A. Gilles, J. K. Hamilton, P. Rebers, and F. Smith, *Anal.*
528 *Chem.*, 1956, **28**, 350-356.
- 529 25.M. M. Bradford, *Anal. Biochem.*, 1976, **72**, 248-254.
- 530 26.R. Lambert, C. Grant, and S. Sauvé, *Sci. Total Environ.*, 2007, **378**, 293-305.
- 531 27.R. Jain, N. Jordan, S. Weiss, H. Foerstendorf, K. Heim, R. Kacker, R. Hübner, H.
532 Kramer, E. D. van Hullebusch, F. Farges, and P. N. L. Lens, *Environ. Sci. Technol.*,
533 2015, **49**, 1713-1720.

- 534 28.Y. Cui, L. Li, N. Zhou, J. Liu, Q. Huang, H. Wang, J. Tian, and H. Yu, *Enzyme*
535 *Microb. Technol.*, 2016, **95**, 185-191.
- 536 29.K. Gai, T. P. Hoelen, H. Hsu-Kim, and G. V. Lowry, *Environ. Sci. Technol.*, 2016,
537 **50**, 3342-3351.
- 538 30.M. R. Eftink, in *Topics in Fluorescence Spectroscopy*, eds. J. R. Lakowicz,
539 Springer, German, 2002, pp. 53-126.
- 540 31.T. L. Hill,. *Cooperativity Theory in Biochemistry: Steady-state and Equilibrium*
541 *Systems*, Springer Science & Business Media, 2013.
- 542 32.L. Zhu, H. Qi, Y. Kong, Y. Yu, and X. Xu, *Bioresour. Technol.*, 2012, **124**, 455-
543 459.
- 544 33.J. Schmitt, and H. C. Flemming, *Int. Biodeterior. Biodegradation*, 1998, **41**, 1-11.
- 545 34.X. Wei, L. Fang, P. Cai, Q. Huang, H. Chen, W. Liang, and X. Rong, *Environ.*
546 *Pollut.*,2011, **159**, 1369-1374.
- 547 35.X. Sun, S. Wang, X. Zhang, J. Chen, X. Li, B. Gao, and Y. Ma, *J. Colloid*
548 *Interface Sci.*, 2009, **335**, 11-17.
- 549 36.K. Kavita, A. Mishra, and B. Jha, *Biofouling*, 2011, **27**, 309-317.
- 550 37.Z. Liang, W. Li, S. Yang, and P. Du, *Chemosphere*, 2010, **81**, 626-632.
- 551 38.P. V. Bramhachari, P. B. K. Kishor, R. Ramadevi, R. Kumar, B. R. Rao, and S. K.
552 Dubey, *J. Microbiol. Biotechnol.*, 2007, **17**, 44-51.
- 553 39.K. Kavita, V. K. Singh, A. Mishra, B. Jha, *Carbohydr. Polym.*, 2014, **101**, 29-35.

- 554 40.B. Lartiges, S. Deneux-Mustin, G. Villemin, C. Mustin, O. Barres, M. Chamerois,
555 B. Gerard, and M. Babut, *Water Res.*, 2001, **35**, 808-816.
- 556 41.W. D. Burgos, J. T. McDonough, J. M. Senko, G. Zhang, A. C. Dohnalkova, S.
557 D. Kelly, Y. Gorby, and K. M. Kemner, *Geochim. Cosmochim. Acta*, 2008, **72**,
558 4901-4915.
- 559 42.X. Pan, J. Liu, and D. Zhang, *Colloids Surf. B Biointerfaces*, 2010, **80**, 103-106.
- 560 43.W. Song, X. Pan, S. Mu, D. Zhang, X. Yang, and D. J. Lee, *Bioresour. Technol.*,
561 2014, **160**, 119-122.
- 562 44.G. Guibaud, E. van Hullebusch, and F. Bordas, *Chemosphere*, 2006, **64**, 1955-
563 1962.
- 564 45.J. Buffle, K. J. Wilkinson, S. Stoll, M. Filella, and J. Zhang, *Environ. Sci.*
565 *Technol.*,1998, **32**, 2887-2899.
- 566 46.U. Gupta, H. B. Agashe, N. K. Jain, *J. Pharm Pharm. Sci.*, 2007, **10**, 358-367.
- 567 47.R. Jain, N. Jordan, S. Tsushima, R. Hübner, S. Weiss and P. Lens, *Environ. Sci.:*
568 *Nano*, 2017, **4**, 1054-1063.
- 569 48.A. M. E. Badawy, T. P. Luxton, R. G. Silva, K. G. Scheckel, M. T. Suidan, and T.
570 M. Tolaymat, *Environ. Sci. Technol.*, 2010, **44**, 1260-1266.
- 571 49.K. Ikuma, A. S. Madden, A. W. Decho and B. L. Lau, *Environ. Sci.: Nano*, 2014,
572 **1**, 117-122.
- 573 50.S. S. Khan, A. Mukherjee, and N. Chandrasekaran, *Water Res.*, 2011, **45**, 5184-

574 5190.

575 51.N. Joshi, B. T. Ngwenya, and C. E. French, *J. Hazard. Mater.*, 2012, **241**, 363-

576 370.

577 52.N. C. Johnson, S. Manchester, L. Sarin, Y. Gao, I. Kulaots, and R. H. Hurt,

578 *Environ. Sci. Technol.*, 2008, **42**, 5772-5778.

579 53.N. T. Prakash, N. Sharma, R. Prakash, K. K. Raina, J. Fellowes, C. I. Pearce, J.

580 R. Lloyd, and R. A. D. Pattrick, *Biotechnol. Lett.* 2009, **31**, 1857-1862.

581 54.C. Pearce, R. A. D. Pattrick, N. Law, J. M. Charnock, V. S. Coker, J. W. Fellowes,

582 R. S. Oremland, and J. R. Lloyd, *Environ. Technol.* 2009, **30**, 1313–1326.